The EUMETSAT Network of Satellite Application Facilities

H SAF
Support to Operational Hydrology and Water Management

Italian Meteorological Service

Italian Department of Civil Defence

Algorithm Theoretical Definition Document (ATDD) for product

SN-OBS-4 - Snow water equivalent by MW radiometry

ZAMG
Zentralanstalt für Meteorologie und Geodynamik

TU WIEN
Vienna University of Technology
Institut für Photogrammetrie und Fernerkundung

RMI
Royal Meteorological Institute of Belgium

European Centre for Medium-Range Weather Forecasts

Finnish Meteorological Institute

SYKE
Finnish Environment Institute

TKK
Helsinki University of Technology

Météo-France

LATMOS
CNRS Laboratoire Atmosphères, Milieux, Observations Spatiales

CESBIO
CNRS Centre d'Etudes Spatiales de la BIOsphere

bfg Bundesanstalt für Gewässerkunde
Bundesanstalt für Gewässerkunde

OMSZ
Hungarian Meteorological Service

ISAC
CNR - Istituto Scienze dell'Atmosfera e del Clima

Università di Ferrara

Institute of Meteorology and Water Management

NMA
Romania National Meteorological Administration

SHMÚ
Slovak Hydro-Meteorological Institute

METEOROLOJİ
Turkish State Meteorological Service

Middle East Technical University

İSTANBUL TEKNİK ÜNİVERSİTESİ
Istanbul Technical University

50.Yıl
Anadolu University

30 May 2010

Algorithm Theoretical Definition Document ATDD-13
Product SN-OBS-4
Snow water equivalent by MW radiometry

INDEX

List of Tables

List of Figures

Acronyms

AMSR-E	Advanced Microwave Scanning Radiometer for EOS (on EOS-Aqua)
ATDD	Algorithms Theoretical Definition Document
AU	Anadolu University (in Turkey)
BfG	Bundesanstalt für Gewässerkunde (in Germany)
CAF	Central Application Facility (of EUMETSAT)
CESBIO	Centre d'Etudes Spatiales de la BIOsphere (of CNRS, in France)
CM-SAF	SAF on Climate Monitoring
CNMCA	Centro Nazionale di Meteorologia e Climatologia Aeronautica (in Italy)
CNR	Consiglio Nazionale delle Ricerche (of Italy)
CNRS	Centre Nationale de la Recherche Scientifique (of France)
DEM	Digital Elevation Model
DMSP	Defence Meteorological Satellite Program
DPC	Dipartimento Protezione Civile (of Italy)
DWD	Deutscher Wetterdienst
ECMWF	European Centre for Medium-range Weather Forecasts
EOS	Earth Observing System (*Terra*, *Aqua*, *Aura*)
EUM	Short for EUMETSAT
EUMETCast	EUMETSAT's Broadcast System for Environmental Data
EUMETSAT	European Organisation for the Exploitation of Meteorological Satellites
FMI	Finnish Meteorological Institute
FTP	File Transfer Protocol
GEO	Geostationary Earth Orbit
GRAS-SAF	SAF on GRAS Meteorology
GTOPO	Global digital elevation model (U.S. Geological Survey)
H-SAF	SAF on Support to Operational Hydrology and Water Management
HUT	Helsinki University of Technology (same as TKK)
IFOV	Instantaneous Field Of View
IMWM	Institute of Meteorology and Water Management (in Poland)
IPF	Institut für Photogrammetrie und Fernerkundung (of TU-Wien, in Austria)
IR	Infra Red
IRM	Institut Royal Météorologique (of Belgium) (alternative of RMI)
ISAC	Istituto di Scienze dell'Atmosfera e del Clima (of CNR, Italy)
ITU	İstanbul Technical University (in Turkey)
LATMOS	Laboratoire Atmosphères, Milieux, Observations Spatiales (of CNRS, in France)
LEO	Low Earth Orbit
LSA-SAF	SAF on Land Surface Analysis
Météo France	National Meteorological Service of France
METU	Middle East Technical University (in Turkey)
MW	Micro Wave
NASA	National Aeronautical and Space Administration (in USA)
NMA	National Meteorological Administration (of Romania)
NOAA	National Oceanic and Atmospheric Administration (Agency and satellite)
NWC	Nowcasting
NWC-SAF	SAF in support to Nowcasting & Very Short Range Forecasting
NWP	Numerical Weather Prediction
NWP-SAF	SAF on Numerical Weather Prediction
O3M-SAF	SAF on Ozone and Atmospheric Chemistry Monitoring
OMSZ	Hungarian Meteorological Service
OSI-SAF	SAF on Ocean and Sea Ice
Pixel	Picture element

PUM	Product User Manual
PVR	Product Validation Report
REP-3	H-SAF Products Validation Report
RMI	Royal Meteorological Institute (of Belgium) (alternative of IRM)
RMSE	Root Mean Square Error
SAF	Satellite Application Facility
SCA	Snow Covered Area
SD	Snow Depth
SHMÚ	Slovak Hydro-Meteorological Institute
SSM/I	Special Sensor Microwave / Imager (on DMSP up to F-15)
SSMIS	Special Sensor Microwave Imager/Sounder (on DMSP starting with S-16)
STD	Standard Deviation
SVRR	System Validation Results Review
SWE	Snow Water Equivalent
SYKE	Suomen ympäristökeskus (Finnish Environment Institute)
TKK	Teknillinen korkeakoulu (Helsinki University of Technology)
TSMS	Turkish State Meteorological Service
TU-Wien	Technische Universität Wien (in Austria)
UniFe	University of Ferrara (in Italy)
VIS	Visible
ZAMG	Zentralanstalt für Meteorologie und Geodynamik (of Austria)

1. The EUMETSAT Satellite Application Facilities and H-SAF

The "*EUMETSAT Satellite Application Facility on Support to Operational Hydrology and Water Management (H-SAF)*" is part of the distributed application ground segment of the "*European Organisation for the Exploitation of Meteorological Satellites (EUMETSAT)*". The application ground segment consists of a "*Central Application Facility (CAF)*" and a network of eight "*Satellite Application Facilities (SAFs)*" dedicated to development and operational activities to provide satellite-derived data to support specific user communities. See ***Fig. 01***.

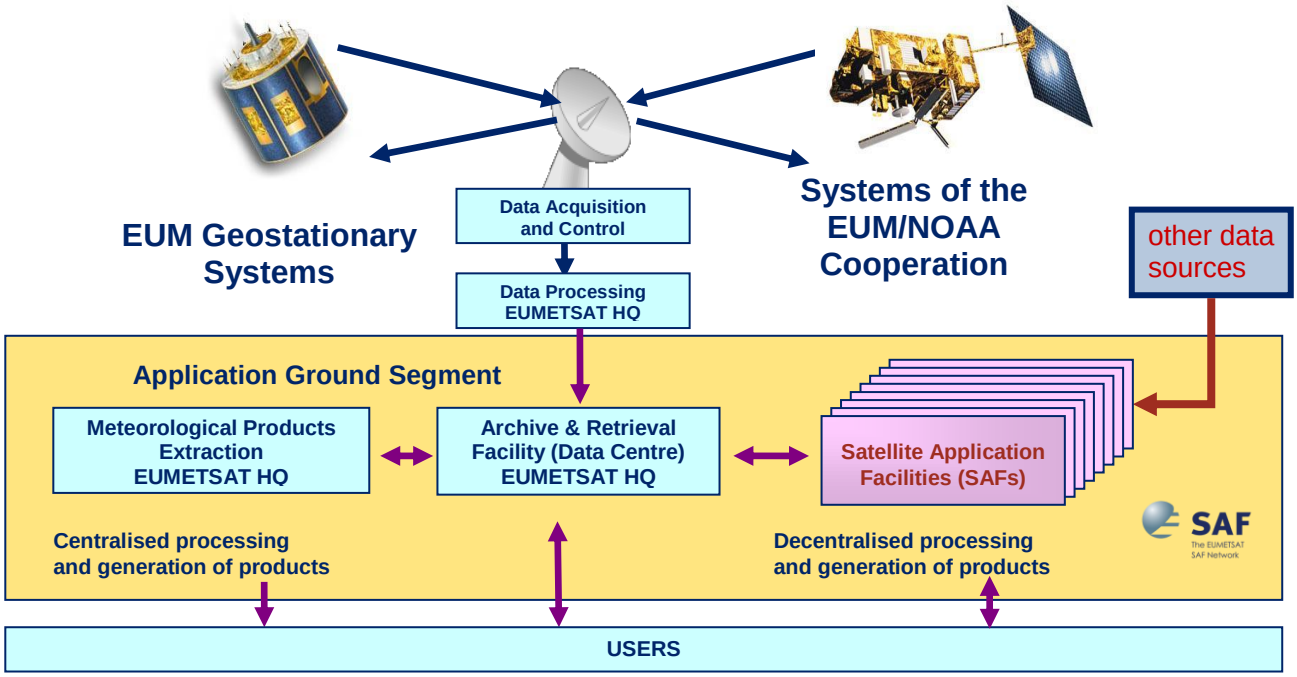

Fig. 01 - Conceptual scheme of the EUMETSAT application ground segment.

Fig. 02 reminds the current composition of the EUMETSAT SAF network (in order of establishment).

NWC SAF	OSI SAF	O3M SAF	CM SAF	NWP SAF	GRAS SAF	LSA SAF	H SAF
Nowcasting & Very Short Range Forecasting	Ocean and Sea Ice	Ozone & Atmospheric Chemistry Monitoring	Climate Monitoring	Numerical Weather Prediction	GRAS Meteorology	Land Surface Analysis	Operational Hydrology & Water Management

Fig. 02 - Current composition of the EUMETSAT SAF network (in order of establishment).

The H-SAF was established by the EUMETSAT Council on 3 July 2005; its Development Phase started on 1st September 2005 and ends on 31 August 2010. The list of H-SAF products is shown in ***Table 01.***

Table 01 - List of H-SAF products

Code	Acronym	Product name
H01	PR-OBS-1	Precipitation rate at ground by MW conical scanners (with indication of phase)
H02	PR-OBS-2	Precipitation rate at ground by MW cross-track scanners (with indication of phase)
H03	PR-OBS-3	Precipitation rate at ground by GEO/IR supported by LEO/MW
H04	PR-OBS-4	Precipitation rate at ground by LEO/MW supported by GEO/IR (with flag for phase)
H05	PR-OBS-5	Accumulated precipitation at ground by blended MW and IR
H06	PR-ASS-1	Instantaneous and accumulated precipitation at ground computed by a NWP model
H07	SM-OBS-1	Large-scale surface soil moisture by radar scatterometer
H08	SM-OBS-2	Small-scale surface soil moisture by radar scatterometer
H09	SM-ASS-1	Volumetric soil moisture (roots region) by scatterometer assimilation in NWP model
H10	SN-OBS-1	Snow detection (snow mask) by VIS/IR radiometry
H11	SN-OBS-2	Snow status (dry/wet) by MW radiometry
H12	SN-OBS-3	Effective snow cover by VIS/IR radiometry
H13	SN-OBS-4	Snow water equivalent by MW radiometry

2. Introduction to product SN-OBS-4

2.1 Sensing principle

Product SN-OBS-4 (*Snow water equivalent by MW radiometry*) is fundamentally based on the AMSR-E microwave radiometer being flown on EOS-Aqua. In case of failure of AMSR-E or of EOS-Aqua, SSM/I and SSMIS flown on the DMSP satellites will be used (with much worse resolution). These conical scanners provide images with constant zenith angle, that implies constant optical path in the atmosphere and homogeneous impact of the polarisation effects (see ***Fig. 03***).

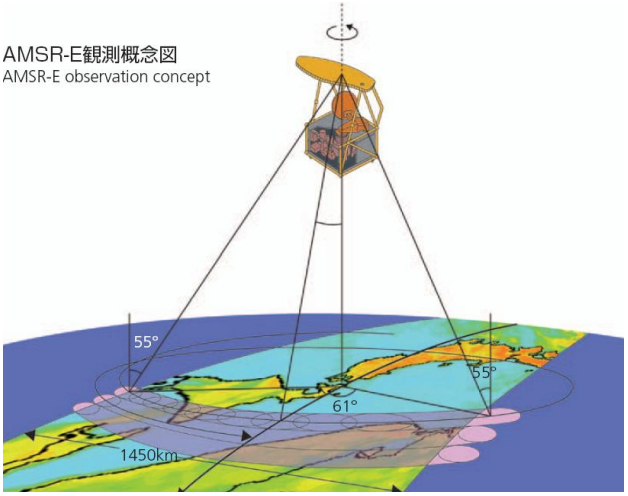

Fig. 03 - Geometry of conical scanning for AMSR-E.

Also, conical scanning provides constant resolution across the image, though changing with frequency. It is noted that the IFOV is elliptical, with major axis elongated along the viewing direction and the minor axis along-scan, approximately 2/3 of the major. As for the 'pixel', i.e. the area subtended as a consequence of the bi-dimensional sampling rate, the sampling distance along the satellite motion, i.e. from scan line to scan line, is invariably 10 km, dictated by the satellite velocity on the ground and the scan rate. Along scan, the sampling rate is 10 km for all channels except 89 GHz where is 5 km.

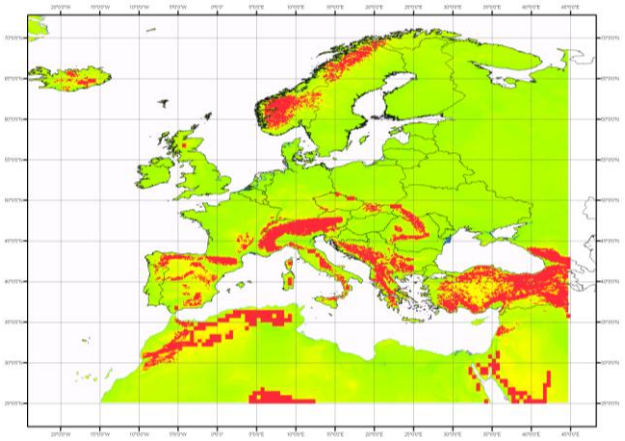

Fig. 04 - Mask flat/forested versus mountainous regions.

The SN-OBS-4 product is actually the result of an assimilation process. The basic (very sparse) ground network of stations performing snow depth observation provides a first guess field that is converted into MW brightness temperatures by an emission model that also accounts for forests. The assimilation process forces the first guess field to optimally match the AMSR-E brightness temperatures.

The retrieval algorithm is somewhat different for flat or forested area and for mountainous regions. SN-OBS-4 is generated in Finland by FMI and in Turkey by TSMS. The products from FMI and from TSMS both cover the full H-SAF area, but thereafter are merged at FMI by blending the information on flat/forested areas from the FMI product and that one on mountainous areas from the TSMS product, according to the mask shown in ***Fig. 04***.

For more information, please refer to the Products User Manual (specifically, volume PUM-13).

2.2 Main operational characteristics

The operational characteristics of SN-OBS-4 are discussed in PUM-13. Here are the main highlights.

The horizontal resolution (Δx). For MW conical scanners the IFOV is constant, but depends on the frequency channels utilised for building the product. The current algorithm utilises the two frequencies 18.7 and 36.5 GHz, thus the resolution is that one of AMSR-E at 18.7 GHz, i.e. ~ 20 km. Sampling is made at 0.25° intervals. Conclusion:

- resolution: $\Delta x \sim 20$ km - sampling distance: ~ 20 km.

The *observing cycle (Δt)*. AMSR-E is available only on one satellite, and its swath is 1450 km, thus in principle provides global coverage every 24 h. Conclusion:

- observing cycle: $\Delta t = 24$ h.

The *timeliness (δ)*. For a product resulting from multi-temporal analysis disseminated at a fixed time of the day, the time of observation may change pixel by pixel (some pixel may have been cloud-free early in the time window, e.g. in the early morning, thus up to 12-h old at the time of dissemination; some very recently, just before product dissemination in the late afternoon). Thus the average timeliness is:

- timeliness δ ~ 6 h.

The *accuracy* is evaluated *a-posteriori* by means of the validation activity. See Product Validation Report PVR-13.

2.3 Architecture of the product generation chain

The architecture of the SN-OBS-4 product generation chain is shown in ***Fig. 05***.

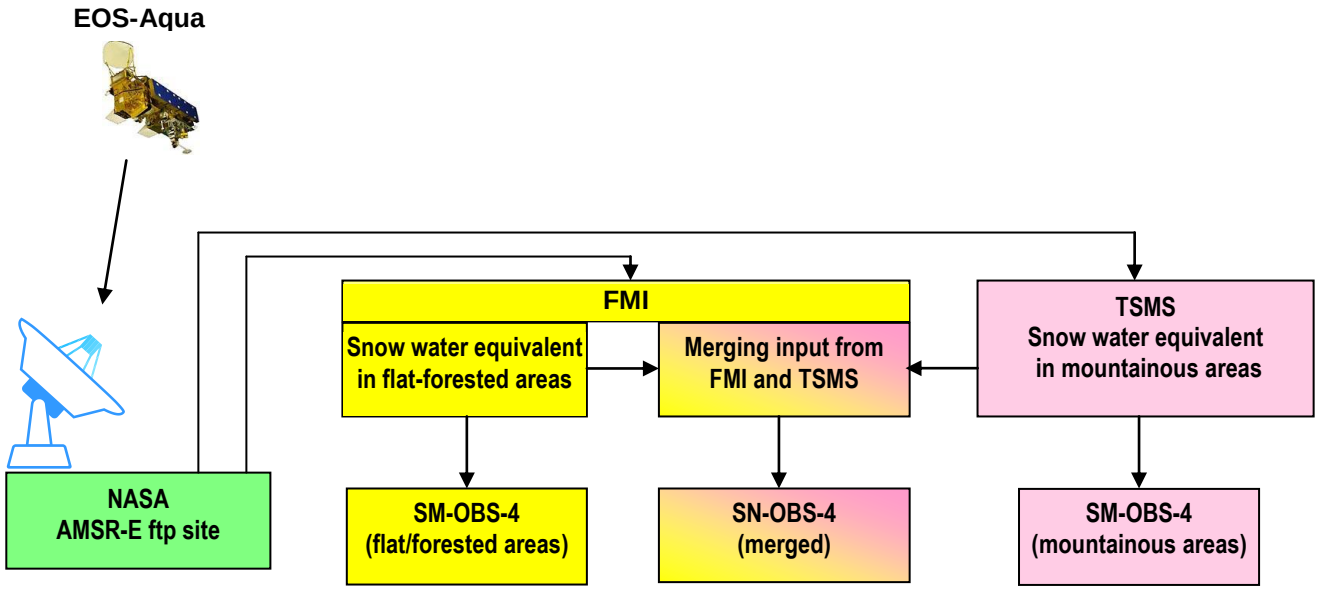

Fig. 05 - Conceptual architecture of the SN-OBS-4 chain.

It is noted that the satellite data are acquired from the NASA EOS-Aqua AMSR-E FTP site. The product is generated both at FMI and at TSMS. The FMI product is tuned to flat/forested areas, that one from TSMS is tuned to mountainous areas. The TSMS data are delivered to FMI, that implements the merging of the two products according to the mask shown in Fig. 04.

Currently, the products are held on the TSMS server (mountainous areas) and on the FMI and CNMCA servers (both flat/forested areas and merged). Eventually, only the merged product will be disseminated through EUMETCast.

2.4 Product development team

Names and coordinates of the main actors for SN-OBS-4 algorithm development and integration are listed in ***Table 02***.

Table 02 - Development team for product SN-OBS-4

Jouni Pulliainen (Leader)	Finnish Meteorological Institut (FMI)	Finland	jouni.pulliainen@fmi.fi
Panu Lahtinen			panu.lahtinen@fmi.fi
Matias Takala			matias.takala@fmi.fi
Juha-Petri Karna	Finnish Environment Institute (SYKE)		juha-petri.karna@ymparisto.fi
Ali Ünal Sorman (Co-leader)	Middle East Technical University (METU)	Turkey	sorman@metu.edu.tr
Ozgur Beser			beser@metu.edu.tr
Zuhal Akyurek			zakyurek@metu.edu.tr

3. Processing concept

The processing concepts for product SN-OBS-4 applied in Finland (FMI) and Turkey (METU) are very similar. They are recorded independently.

3.1 Flat and forested areas [TKK]

Fig. 06 shows the flow diagram of the assimilation method, limited to the case of AMSR-E observations that are currently used for snow water equivalent retrieval in flat/forested areas.

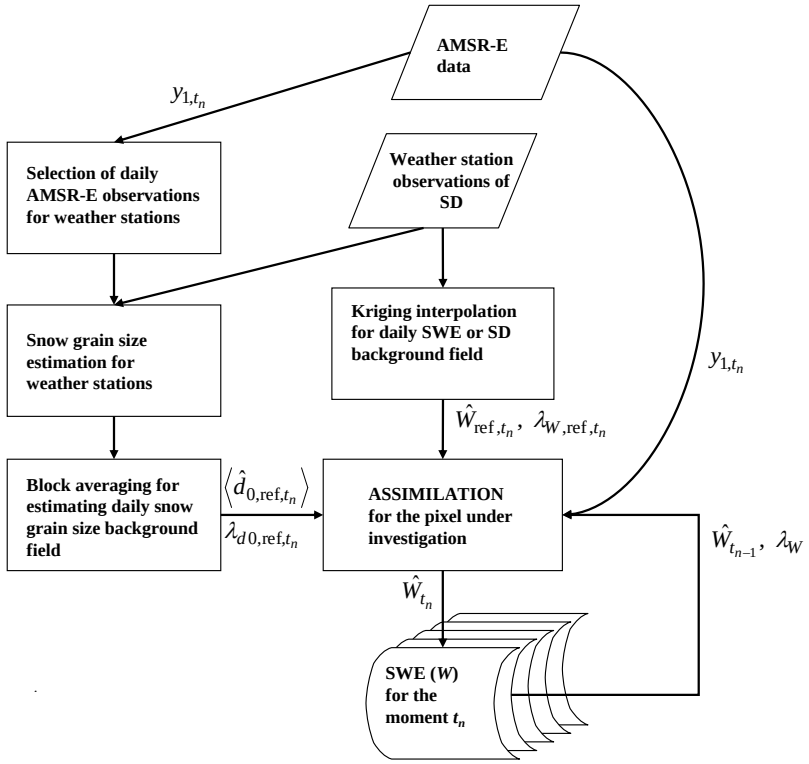

Fig. 06 - Flow diagram of the assimilation method in the case of AMSR-E observations in flat/forested areas.

3.2 Mountainous regions [METU]

Fig. 07 shows the flow diagram of the assimilation method, limited to the case of AMSR-E observations that are currently used for snow water equivalent retrieval in mountainous regions.

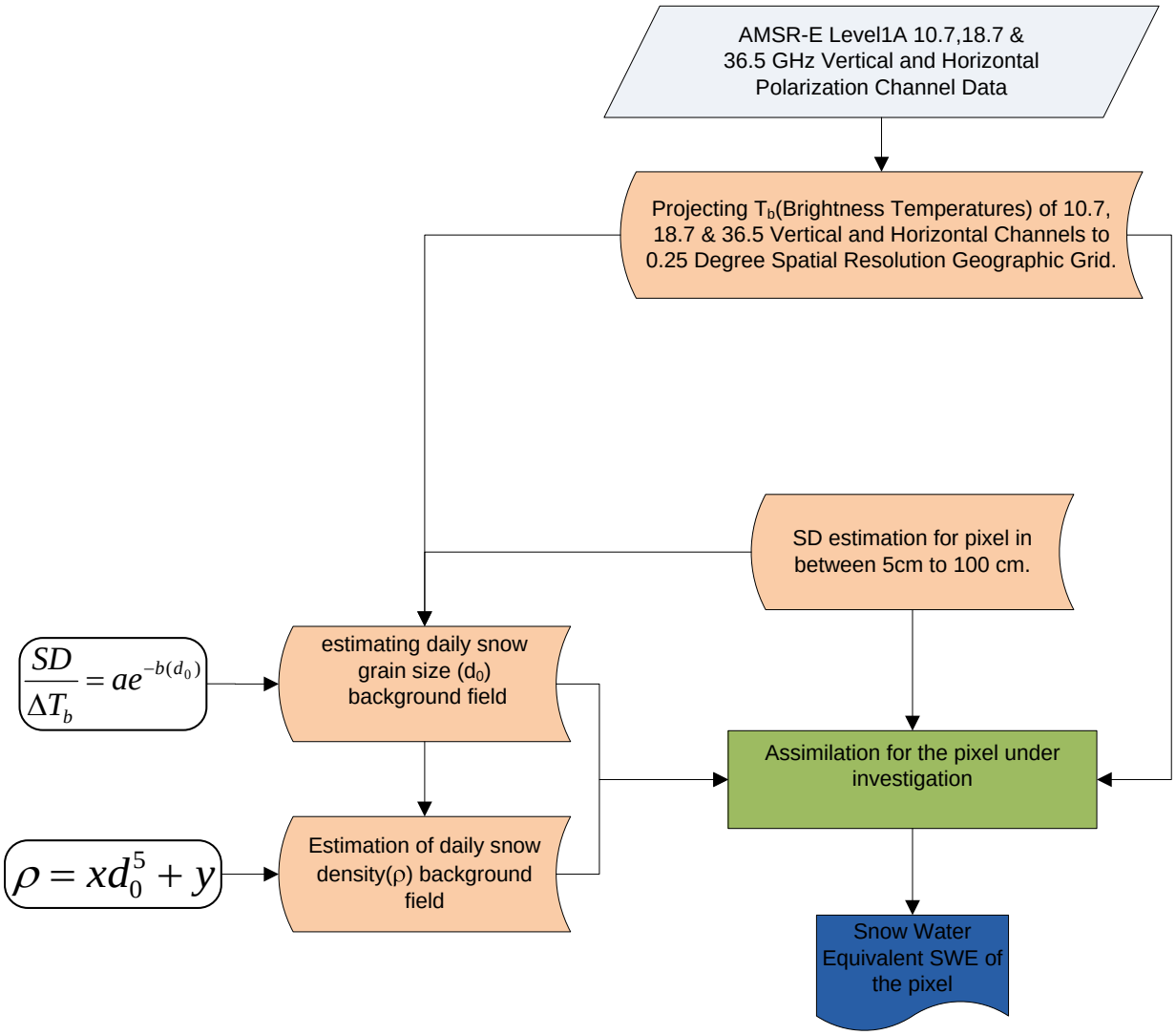

Fig. 07 - Flow diagram of the assimilation method in the case of AMSR-E observations in mountainous areas.

4. Algorithms description

4.1 Flat and forested areas [TKK]

The HUT snow emission model

The HUT snow emission model describes the space-borne observed microwave brightness temperature as a function of snow pack characteristics and by considering the effects of atmosphere, forest canopy and land cover category (fractions of open and forested areas). A detailed description of the model and its performance is given by Pulliainen et al. 1999. The emission from a snow pack is modeled by applying the Delta-Eddington-approximation to the radiative transfer equation (considering the magnitude of forward scatter by an empirical coefficient). The multiple reflections from snow-ground and snow-air boundaries are included using a non-coherent approach and the effect of forest canopy (transmissivity and emission) is included by employing an empirical model (Kruopis et al. 1999). Finally, the transmissivity and emission contributions of the atmosphere are included using a statistical atmospheric model (Pulliainen et al. 1993).

The input parameters of the HUT model include the snow pack characteristics (depth, density, effective grain size and temperature), soil properties (temperature, dielectric constant and effective rms height variation), forest canopy characteristics (stem volume/biomass) and near-surface air temperature dependent atmospheric emission and transmissivity contributions. The model formulation and its inversion are described in detail in (Pulliainen and Hallikainen 2001). ***Table 03*** summarizes typical values of adjustable model parameters as the HUT model is applied to the inversion of space-borne data. A brief summary of the inversion technique follows here.

Table 03 - Pre-fixed HUT snow emission model parameter values for Northern Eurasia

Parameter	Value
Mean effective snow grain size, $\langle d_0 \rangle$ (mm)	1.3
Variance of d_0, var(d_0) (mm^2)	1.0
Variance of modeling error, var(ε_t) (K^2)	25
Variance of day-to-day SWE variation, var(W) (mm^2)	25
Snowpack density (g/cm^3)	0.23
Effective soil surface roughness (mm)	3
Temperature, soil/snow/vegetation/near surface air (C °)	-5
Soil dielectric constant	6-1j

Inversion of the snow emission model

Let the vector **y** containing space-borne observed spectral and polarization brightness temperature differences be:

$$y = \begin{bmatrix} y_1 \\ y_2 \end{bmatrix} = \begin{bmatrix} T_{b,19V,obs} - T_{b,37V,obs} \\ T_{b,19V,obs} - T_{b,19,H,obs} \end{bmatrix}, \quad (1)$$

where $T_{b,19V,obs}$ is the brightness temperature observed at a vertically polarized channel (close to) the frequency of 19 GHz. Accordingly, subscript H denotes horizontal polarization and 37 stands for the frequency region of about 37 GHz.

The main snow pack characteristics affecting brightness temperatures at 19 and 37 GHz regions include the snow water equivalent, SWE, denoted here by W and the snow grain size (d_0). Brightness temperature differences according to (1) can be modeled by applying the HUT snow emission model. For simplicity we denote this direct modeling of channel differences by **f**(**x**), where

$$x = \begin{bmatrix} W & d_0 \end{bmatrix}^T \quad (2)$$

and thus

$$y = f(x) + \varepsilon = \begin{bmatrix} f_1(x) \\ f_2(x) \end{bmatrix} + \begin{bmatrix} \varepsilon_1 \\ \varepsilon_2 \end{bmatrix}, \tag{3}$$

where **ε** is the vector of modeling error including the effect of instrument noise and all inaccuracies of modeling. If modeling error is assumed to be non-biased and normally distributed, the conditional probability density of satellite observations **y** as a function of **x** obeys the multidimensional normal distribution, refer to e.g. (Pulliainen and Hallikainen 2001; Pulliainen et al. 2004). Further on, as the Bayes' theorem is applied we can write the expression for the conditional density of snow characteristics **x** taking also into account possible *a priori* information on snow grain size (diameter):

$$\rho(x \mid y) = \rho(W, d_0 \mid y)$$
$$\propto \exp\left\{ -\frac{1}{2}\left[y - f(W,d_0)\right]^T C^{-1}\left[y - f(W,d_0)\right] - \frac{1}{2\mathrm{var}(d_{0,\mathrm{ref}})}\left(\hat{d}_{0,\mathrm{ref}} - d_0\right)^2 \right\}, \tag{4}$$

where *a priori* information suggests that d_0 is a normally distributed random variable with the expected value $\hat{d}_{0,\mathrm{ref}}$ and variance var($d_{0,\mathrm{ref}}$). **C** is the covariance matrix of modeling errors.

The maximum likelihood modeled estimate on W and d_0 is obtained by searching the global minimum of the absolute value of the exponent term given in (4), i.e. the minimum of the cost function $J(W, d_0)$:

$$J(W,d_0) = \left\{ \frac{1}{2}\left[y - f(W,d_0)\right]^T C^{-1}\left[y - f(W,d_0)\right] + \frac{1}{2\mathrm{var}(d_{0,\mathrm{ref}})}\left(\hat{d}_{0,\mathrm{ref}} - d_0\right)^2 \right\}. \tag{5}$$

Thus, the maximum likelihood estimate on SWE and grain size, $\hat{x} = \begin{bmatrix} \hat{W} & \hat{d}_0 \end{bmatrix}^T$, must satisfy

$$\frac{\partial J(W = \{\hat{W}, d_0 = \hat{d}_0)}{\partial W} = 0 \qquad \left\{ \frac{\partial J(W = \{\hat{W}, d_0 = \hat{d}_0)}{\partial d_0} 0 \right\}. \tag{6}$$

As the HUT snow emission model is non-linear, the global minimum of (5) must be searched iteratively. If the correlation between modeling errors ε_1 and ε_2 is assumed to be close to zero (or unknown), the error covariance matrix **C** in (5) is a diagonal matrix and (5) leads to a common least squares problem:

$$\left\{ \sum_{i=1}^{2} \frac{1}{\mathrm{var}(\varepsilon_i)}\left[y_i - f_i(x)\right]^2 + \frac{1}{\mathrm{var}(d_{0,ref})}\left[\hat{d}_{0,ref} - d_0\right]^2 \right\}. \tag{7}$$

If *a priori* information on the temporal changes of SWE is available, this information can be also used to regulate the algorithm. In practice, this is reasonable when a time-series of brightness temperature observations are analyzed. In that case (7) modifies to:

$$\left\{ \sum_{i=1}^{2} \frac{\left[y_i - f_i(x)\right]^2}{\mathrm{var}(\varepsilon_i)} + \frac{\left[\hat{d}_{0,ref} - d_0\right]^2}{\mathrm{var}(d_{0,ref})} + \frac{\left[W_{t-1} - W_t\right]^2}{\mathrm{var}(W_t)} \right\}, \tag{8}$$

where W_{t-1} denotes the level of SWE on the day prior to the day under investigation and the variance of day-to-day changes in SWE is denoted by var(W_t) .

Formulation (8) defines the inversion algorithm applied in this investigation. The algorithm considers the effect of possibly available *a priori* information. This is performed by weighing the satellite data (the first term of (8)) and reference information on snow grain size with their estimated statistical accuracy. If *a priori* information on SWE is available and that information has a Gaussian distributed uncertainty, it can be considered by summing it similarly to the d_0 term in (7) and (8). Hence, (7) and (8) actually formulate the solution of the assimilation problem discussed next.

Assimilation technique

The data-assimilation technique applies a single channel difference, y_1 of (1). That is, the brightness temperature difference between vertically polarized AMSR-E (SSM/I) channels of 18.7 (19.0) and 36.5 (37.0) GHz is used. This channel difference is the most commonly used index to derive SWE or SD (Chang et al. 1987). Again, the brightness temperature difference between the two channels is modelled by the HUT snow emission model. A maximum *a posteriori* probability of SWE or SD, when certain values of brightness temperatures are observed, is searched through the iterative inversion procedure analogously to (7). Ground-based (interpolated) SWE or SD value is employed as statistical *a priori* information. When meteorological synoptic SD observations are employed as a source of *a priori* information, the obtained SD estimates are converted to SWE estimates by multiplying them with snow density values that are regional and seasonal averages obtained from snow climatology (in case of testing the algorithm for Finland the climatology is obtained from snow course observation data).

SWE (or SD) estimates for all locations are interpolated from distributed synoptic observations and these values are applied as *a priori* estimates on SWE, when the scene brightness temperature model is fitted to space-borne observations by optimizing the value of SWE. In the fitting procedure, the *a priori* SWE-value is weighed with its modelled statistical uncertainty determined using spatial data analysis techniques (Kriging interpolation). As well, the radiometer data is weighed with the estimated accuracy of brightness temperature modelling. In that case, weighing factors are determined by analysing how well the brightness temperature model describes the radiometer observations at the locations of synoptic observations for the day under investigation (in that phase the consideration of snow grain size is included in the algorithm). The inclusion of (interpolated) SWE estimates as *a priori* data regulates the optimization procedure. Hence, the assimilation can be performed using a single channel difference y_1 of (9), i.e. using the channel difference that has the highest correlation with SWE.

We can write the assimilation algorithm as a three-stage optimization procedure (see Fig. 06 for the illustration).

The first phase of the algorithm is the estimation of effective snow grain size at the locations of reference stations, for which SD is observed. The grain size estimation is conducted by fitting the modeled brightness temperature difference into the brightness temperature difference observed by the instrument:

$$\left(y_1 - f_1(\rho\rho D, d_0)\right)^2 0\,, \tag{9}$$

where D is the observed snow depth and ρ is snow density (note that $W=D\rho$). ρ is treated as a constant (using a temporal mean value from monthly snow climatology).

The procedure (9) is repeated for all reference stations for the day under investigation. The snow grain size for an arbitrary location *(x, y)* is then assumed to be equal to the mean of snow grain size estimated at its near-by-stations:

$$\left\langle \hat{d}_{0,\mathrm{ref}} \right\rangle = \frac{1}{M}\sum_{j=1}^{M} \hat{d}_{0,\mathrm{ref},j}\,, \tag{10}$$

where M is the number of reference stations in the neighbourhood of the location under investigation. Nine closest stations are used in case of testing for Finland and four closest for Eurasia. In Finland, the maximum distance between neighbouring stations is less than 100 km, but in the Eurasian case this distance exceeds to almost 1000 km, which causes the low value, M = 4.

According to (10), the standard deviation of the effective snow grain size is estimated by

$$\lambda_{d0,\mathrm{ref}} = \sqrt{\frac{1}{M-1}\sum_{j=1}^{M}\left(\hat{d}_{0,\mathrm{ref},j} - \left\langle \hat{d}_{0,\mathrm{ref}} \right\rangle\right)^2}\,. \tag{11}$$

The second stage of the algorithm is the determination of SWE or SD estimate and its standard deviation for the location under investigation *(x, y)* from a set of distributed ground-based observations. Kriging interpolation (ordinary Kriging) is applied to synoptic SD observations, and SWE is estimated

from the SD-values by multiplying them with snow density reference information. In contrast to block averaging of (10), the Kriging interpolation takes into account the spatial autocorrelation of snow depth (the required semivariogram is estimated from the discrete SD observations). The resulting estimates are:

- Interpolated SWE estimate $\hat{W}_{\text{ref}}$ (or SD estimate) for the location under investigation *(x, y)*.
- Standard deviation of the interpolated SWE estimate $\lambda_{W,\text{ref}}$, i.e. the statistical accuracy of the interpolated SWE estimate for the location *(x, y)* or alternatively the same value for the SD estimate $\lambda_{D,\text{ref}}$.

The third phase of the algorithm is the estimation of SWE for the location *(x, y)* at the moment of time (day) *t* by weighing the two data sources by their estimated variances:

$$\left\{\frac{(\,)^2}{\text{var}(\varepsilon_{1,t})}\right\}\left(+\left(\frac{W_t-\hat{W}_{\text{ref},t}}{\lambda_{W,\text{ref},t}}\right)^2+\left(\frac{W_t-\hat{W}_{t-1}}{\lambda_W}\right)^2\right)\text{such as } W_t \geq 0\,\text{mm}. \qquad (12)$$

Alternatively, (12) can be written in terms of snow depth SD. Fig 6.9 shows the general flow chart of the assimilation method indicating how different contributions of (12) are estimated.

The third term in summation is an optional term that regulates the magnitude of day-to-day changes in SWE (λ_W is the standard deviation of day-to-day changes in snow water equivalent). In the first term of (12), the standard deviation of random error in modelled brightness temperature difference $\varepsilon_{1,t}$ is estimated from the estimated standard deviation of effective snow grain size (λ, see (11)) through the linearization of the relation between the brightness temperature and snow grain size:

$$\Delta T_b(W_t,d_0)\approx \Delta T_b(W_t,\langle\hat{d}_{0,\text{ref,t}}\rangle)+\frac{\partial \Delta T_b(W_t,\langle\hat{d}_{0,\text{ref,t}}\rangle)}{\partial d_0}\left(d_0-\langle\hat{d}_{0,\text{ref,t}}\rangle\right)$$

$$\Rightarrow \quad \text{var}(\varepsilon_{1,t})=\text{var}\left(\Delta T_b(W_t,\langle\hat{d}_{0,\text{ref,t}}\rangle)\right)=\left(\frac{\partial \Delta T_b(W_t,\langle\hat{d}_{0,\text{ref,t}}\rangle)}{\partial d_0}\right)^2\lambda^2_{d0,\text{ref,t}} \qquad (13)$$

where $\Delta T_b = y_1$.

Note that var($\varepsilon_{1,t}$) in (13) is a function of SWE (denoted by W_t). When compared to (7) and (8), a major difference arises from the difference in determining the value of the term var($\varepsilon_{1,t}$). When the assimilation algorithm fits the modelled brightness temperature difference into the observed value at the locations of reference station according to (9), the only fitting parameter to be optimized is the effective snow grain size d_0. Hence, the total modelling error evident for every location between the reference stations is reduced to the spatial inaccuracy of effective d_0. As an outcome, the variance of modelling error, var($\varepsilon_{1,t}$) in (12), has to be determined as a function of snow grain size variance by (13).

[Note] SWE mapping has a problem over lakes, because MW instruments may see the liquid water which may lie between ice and snow. As for large lakes (e.g. Ladoga), the amount of snow is considerably less on their area than around them, so the synoptic weather data used as background in assimilation may overestimate the amount of snow. For small lakes with low fractional coverage in a pixel the impact is lower, but the possible accuracy implications need to be studied further.

4.2 Mountainous regions [METU]

Snow emission model

The HUT snow emission model, which is described in section 4.1, is used. Input and output schema of HUT model is given in ***Fig. 08***. Extinction coefficient κ_e used in the original model is based on an experiment done by Hallikainen et al. (1987). He measured properties of 23 snow samples and used 18

of them for determining empirical relationship between extinction coefficient of snow against grain size(d_o) and frequency (f). The obtained empirical relationship is given in equation (14)

$$\kappa_e = 0.0018 f^{2.8} d_o^{2.0} \quad (14)$$

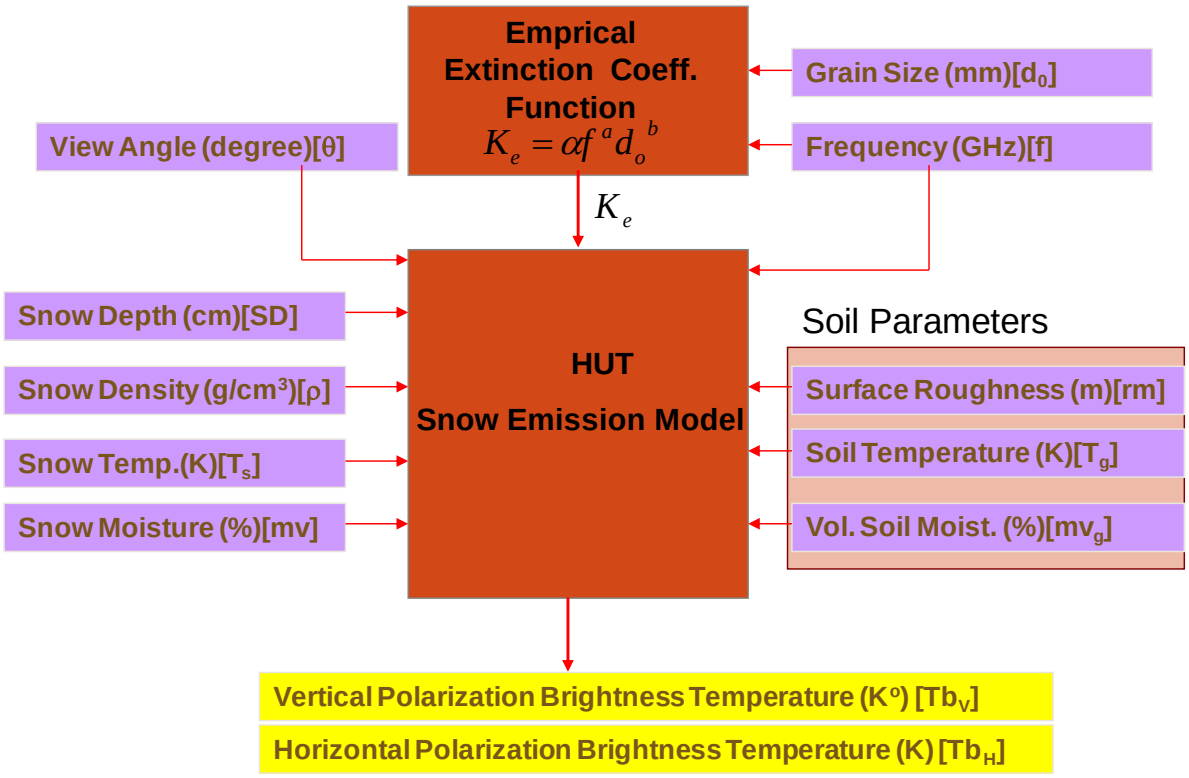

Fig. 08 - Input and output schema of HUT.

Measured 18GHz and 35 GHz extinction coefficients for 18 sample of snow coarse and fitted equation by Hallikainen is given in ***Fig. 09***. R-square of fitted equation for 18GHz is 0.38 and for 35 GHz is 0.85.

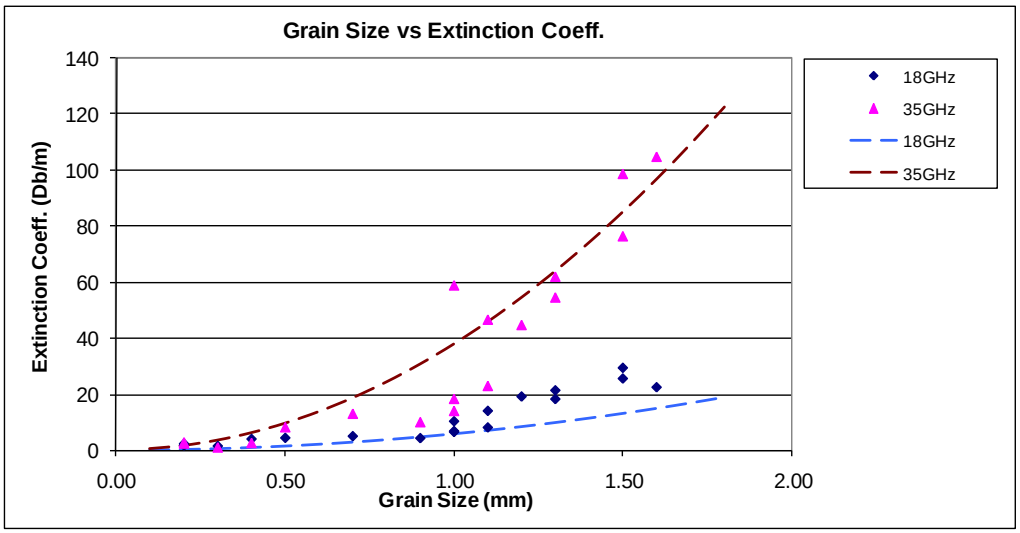

Fig. 09 - Measured extinction coefficients against grain size and fitted equation by Hallikainen et al. (1987).

A new relationship for modeling extinction coefficient based on Hallikainen's data is proposed and given in Equation (15)

$$\kappa_e = 0.08 f^{1.75} d_o^{1.8} \quad (15)$$

Measured 18GHz and 35 GHz extinction coefficients for 18 sample of snow coarse and fitted equation given in (15) is shown in ***Fig. 10***. R-square of fitted equation given in (15) for 18GHz is 0.83 and for 35 GHz is 0.83.

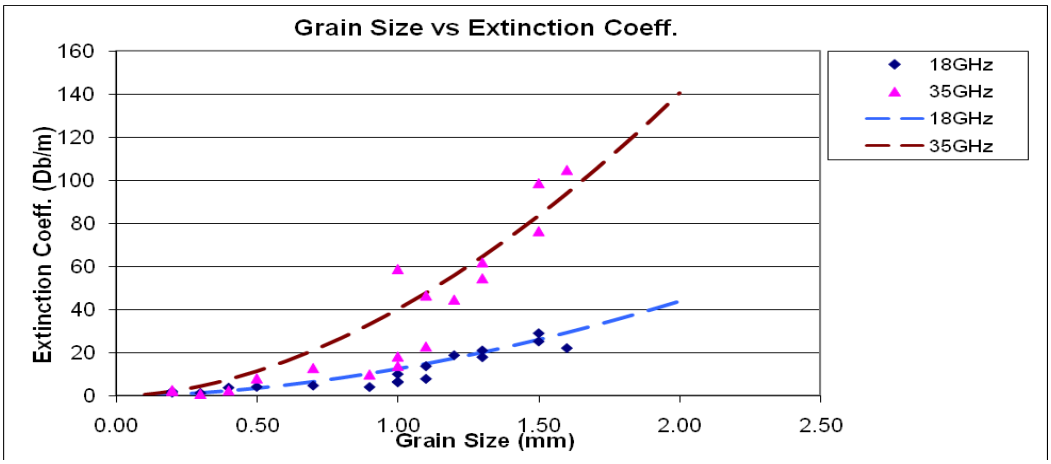

Fig. 10 - Measured extinction coefficients against grain size and fitted equation given in (15).

Performance of proposed extinction coefficient

The snow measurements considered in this study were conducted inside Karasu Basin which is located in the eastern part of Turkey. Snow observations are done by means of Automated Weather Observing Stations (AWOS) which measure snow depth, snow density and snow temperature every 10 minutes. In this study Hacimahmut, Güzelyayla, Ovacik and Cat stations data were used. Elevations of these stations are 1965 m, 2065 m, 2130 m and 2340 m respectively. Period of January 1st to March 15th of years 2003-2007 is analyzed. In this period snow is mostly in dry state.

The input parameters of the HUT model include the snow pack characteristics (snow depth (SD), density (ρ), effective grain size (d_0), and temperature(T_s)), soil properties (temperature(T_g), effective soil surface roughness (RMS) variation(rm), moisture content (mvg)) and near-surface air temperature. ***Table 04*** summarizes typical values of fixed model parameters, as the HUT model is applied to the inversion of space- borne data. For any AMSR-E pixel that includes any AWOS, it is assumed that station measured snow depth and density are homogenous inside that pixel. Therefore only unknown parameter for that pixel is mean grain size of snowpack.

Table 04 - Prefixed HUT model parameters

Parameter	**Value**
Snow Temperature ,T_s	-3°C
Snow moisture content, mv	0%
Effective soil surface roughness, rm	2 mm
Soil temperature, T_g	-1°C
Soil moisture content, mv_g	1%

For every station, HUT model is run by changing grain sizes in order to minimize sum of measured and modeled brightness temperature differences at 18.7 GHz and 36.5 GHz vertical channels. HUT model inversion for calculating grain size is given in ***Fig. 11***. Therefore for every station considered mean grain sizes are calculated.

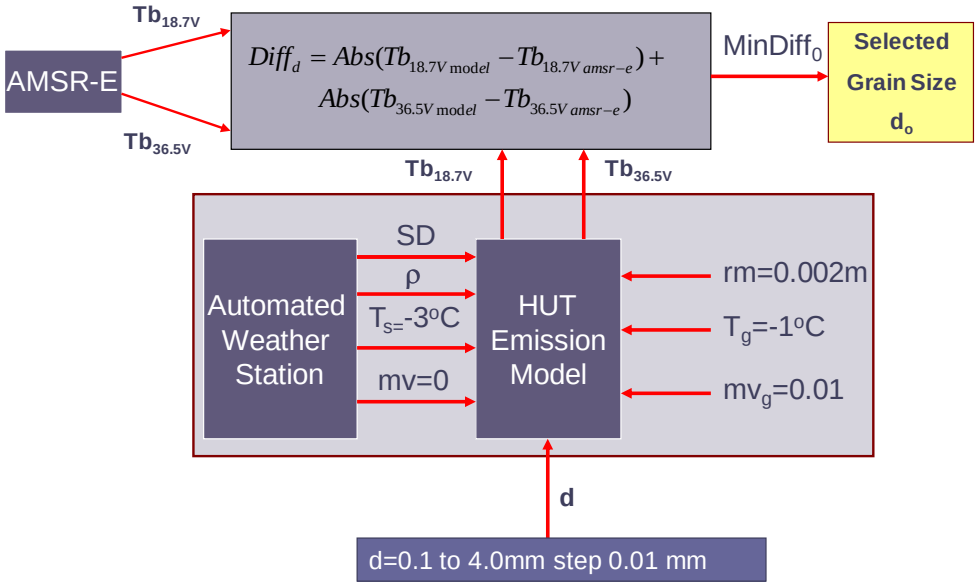

Fig. 11 - Data assimilation schema for obtaining grain size.

Calculated mean of model errors (for selected periods of 2003 to 2007) for two channels namely 18.7 GHz and 36.5 GHz vertical and horizontal polarization is given in ***Table 05***. It is apparent that 36.5 GHz vertically polarized channel is simulated successfully by using both extinction coefficient relationships regarding mean error calculated. At 18.7 GHz channel mean error of proposed relationship is less than half of original one for both horizontal and vertical polarizations.

Table 05 - Mean Model Error (K) of Stations for whole period (2003-2007) at Vertical, Horizontal Polarizations

Band	**Equation (14)**	**Equation (15)**
18.7V	5.75	2.73
18.7H	10.37	3.79
36.5V	0.29	0.46
36.5H	4.48	4.79

Assimilation technique

In order to calculate SWE in each domain pixel one should calculate snow density and snow depth for the particular pixel in interest. Calculation of these two parameters is done by inversion of HUT emission model. Inputs of the HUT model is depicted in Fig. 08 and prefixed values are listed in Table 04. The only unknown parameters are snow depth, snow density and effective grain size of snow layer.

We searched a relationship between grain size, snow depth and brightness temperature difference of vertically polarized channels 18.7 GHZ and 36.5GHz as given in equation (16)

$$\frac{SD}{\Delta T_B} = ae^{b(d_0)} \Rightarrow SD = (ae^{b(d_0)})\Delta T_B \qquad (16)$$

where d_o is grain size; SD is snow depth; $\Delta T_B = T_{B,18.7} - T_{B,36.5}$.

a and b coefficients for each month during dry snow period is searched using calculated grain sizes by HUT. Results for January, February and March is tabulated in ***Table 06***. All three months correlation coefficients are higher than 0.80. It is interesting that a coefficient decreases from January to March where b coefficient increases.

Table 06 - Calculated a and b coefficients for January, February and March using equation (16)

Month	a	b	RMSE	R^2	%95 a	%95 b	Sample Number
January	21.94	-2.844	0.2344	0.8734	19.76, 24.12	-2.966, -2.721	351
February	19.87	-2.666	0.2095	0.912	18.43, 21.31	-2.759, -2.574	341
March	17.14	-2.378	0.3098	0.8289	14.72, 19.57	-2.561, -2.196	141

If we multiply both side of Equation. (16) with snow density and take logarithms equation (17) is obtained. The calculated mean densities using Equation (17) for January, February and March using a and b coefficients are compared by measured densities and the results are given in ***Table 07***.

$$\frac{SD}{\Delta T_B} = ae^{bd_0} \Rightarrow \frac{\rho SD}{\Delta T_B} = \rho ae^{bd_0} \Rightarrow \frac{SWE}{\Delta T_B} = \rho ae^{bd_0}$$
$$\ln(\rho) = \ln(\frac{SWE}{\Delta T_B}) - \ln(a) - bd_0 \quad (17)$$

Table 07 - Calculated and measured snow densities at three AWOS

	JANUARY		FEBRUARY		MARCH	
	CALC.	MEAS.	CALC.	MEAS.	CALC.	MEAS.
GUZELYAYLA	0.25	0.25	0.27	0.27	0.30	0.30
OVACIK	0.22	0.21	0.25	0.24	0.28	0.28
CAT	0.28	0.30	0.28	0.30	0.30	0.32

We searched a relationship between calculated grain sizes and measured densities in the form of Equation (18) keeping the power term to be 5 for each investigated month where grain size is measured in mm and density is in g/cm^3. Calculated x and y coefficients and respective RMSE are presented in ***Table 08***.

$$\rho = xd_0^5 + y \quad (18)$$

Table 08 - Calculated x and y coefficients for equation (18)

Month	x	y	RMSE
JANUARY	-0.04727	0.2797	0.04056
FEBRUARY	-0.03738	0.2871	0.04278
MARCH	-0.01711	0.3015	0.05037

For every pixel, HUT model is run by assuming snow depth from 0.05 m to 1.00 m by 0.05 depth intervals in order to minimize sum of measured and modeled brightness temperature differences at 18.7 GHz and 36.5 GHz vertical channels. During this stage snow grain size is dynamically calculated using Equation (16) with selected empirical coefficients and density is calculated by inserting obtained grain size to Equation (18). As a result the depth value which leads to smallest brightness temperature error is selected as that pixels depth value. Density of that particular pixel is also calculated by Equation (18). SWE of the pixel is assigned as multiplication of calculated snow depth and density.

4.3 Algorithms validation/heritage

4.3.1 Flat and forested areas [TKK]

The algorithms and methods described above have been presented and tested in published peer-reviewed paper, Pulliainen 2006. The method was tested with SSM/I data in Northern Eurasia and in Canada, and with AMSR-E data in Finland. These tests indicate that in 62 % of the cases there was an improvement in the Snow depth estimate when used in Northern Eurasia in the period winter period from November 1993 to April 1994. For Finland the improvement was from 50.2 % (February 2004) to 61.6 % (February 2005) of the cases. The results for the test site in Finland are summarized in ***Table 09***. The described method was also tested semi-operatively in spring 2007 in Eurasia (Kärnä et al. 2007).

The used emission model, HUT emission model, is published in Pulliainen et al. 1999. The emission model has been used by others too, for example in Canada, to retrieve snow water equivalent (Roy et al. 2004).

Table 09 - Quantitative performance of Snow depth and SWE retrieval for a Finnish test site when using interpolation of ground-based measurements and assimilation of satellite data to the interpolation result

	RMSE (mm)		Bias		r^2	
	Snow depth	Snow water equivalent	Snow depth	Snow water equivalent	Snow depth	Snow water equivalent
February 2004, N = 99						
Interpolation	9.8	29.3	- 0.8	- 3.8	0.662	0.418
Assimilation	8.9	28.2	0.4	- 1.3	0.696	0.431
February 2005, N = 235						
Interpolation	13.3	35.9	1.0	- 2.7	0.648	0.578
Assimilation	13.1	35.5	0.9	- 2.8	0.652	0.580

4.3.2 Mountainous regions [METU]

All in-situ measurements conducted in between 2009 October to 2010 March period were compared individually with the corresponding 25x25 km2 AMSR-E footprint. For each measurement location the elevation of the weather station or ground measurement is compared against the AMSR-E pixel median elevation where the measurement falls inside it. If the elevation difference between measurement location and pixel elevation median value is greater than 400 meters that weather station or ground measurement is excluded from validation studies. Elevation range of ground truth data is from 981 meters to 2937 meters.

All the stations used in validation study measure only snow depth. In order to calculate snow water equivalent values for each station average seasonal snow density values were used. The resulting error summary plot of SWE with 148 measurements is shown in ***Fig. 12*** and listed in ***Table 10***. The RMSE of the study is 46.14 mm.

It is obvious that error amount increases when SWE values measured are less than 75 mm and SWE values measured are higher than 175.0 mm. Sensor limitations prevent us to improve accuracy of product for SWE values higher than 150 mm but for SWE values less than 75 mm fine tuning of the algorithm can be considered. It should also be noted that only 3 measurements have been used during validation studies for SWE values less than 50 mm. A new approach considering pixel median elevation is planned to be used in order to modify validation results for SWE values less than 75mm where 10GHz channels will be integrated. In this method, a threshold for pixel median elevation will be determined and below that value a new assimilation schema will be applied. For elevation values higher than specified threshold, existing algorithm will be used.

Table 10 - SWE Validation Study Results Summary for 2009 October-2010 March period

Range mm	Measured SWE mm	Assimilated SWE mm	Standard Deviation mm	Measurement Count	Mean Error mm
0-50	46.77	106.67	11.03	3	59.90
50-75	59.62	99.10	28.70	39	39.49
75-100	86.35	103.78	25.89	32	17.43
100-125	111.30	116.40	23.07	20	5.10
125-150	134.75	96.00	25.70	19	38.75
150-175	163.26	119.21	15.06	14	44.05
175-200	187.15	119.92	9.89	12	67.23
200-225	207.45	164.78	46.06	9	42.67

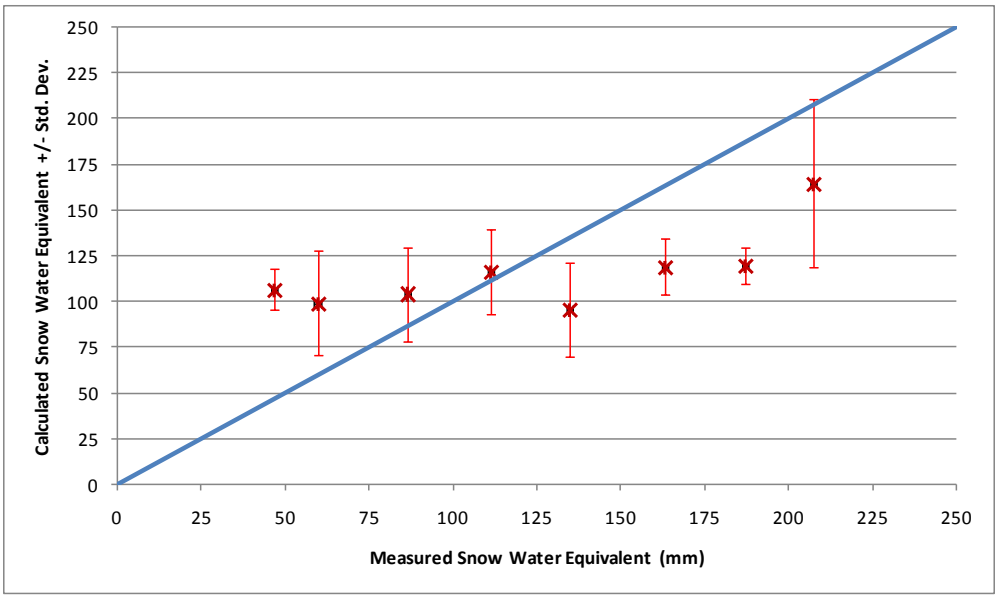

Fig. 12 - SWE Validation Study Results Summary Plot for 2009 October-2010 March period.

5. Merging products for flat/forested and mountainous areas

5.1 Merging according the H-SAF mountain mask

Although the products for flat/forested areas and for mountainous areas generated by FMI and TSMS cover the full H-SAF area, their quality differs in different areas, the product from FMI being tuned for flat/forested areas, that one from TSMS being tuned for mountainous areas. However, a single product is distributed to the users, obtained by merging the two products in such a way that in flat/forested areas the FMI product is captured, and in mountainous areas the TSMS product is captured. The distinction is determined by the "mountain mask" shown in Fig. 03, that was defined by METU.

A mask based on digital elevation model (DEM) was used to separate the mountainous pixels from flat/forested areas. The merging algorithm finds the location of the non-mountainous pixels using this mask. As the spatial sampling of the product is sparse, some of the pixels have mixed case of mountainous and non-mountainous areas. For this reason, the mountain-fraction weighed average of the two SWE values is used.

The flow chart for calculating the look-up table is shown in ***Fig. 13*** and the merging procedure in ***Fig. 14*** (Ertürk 2009).

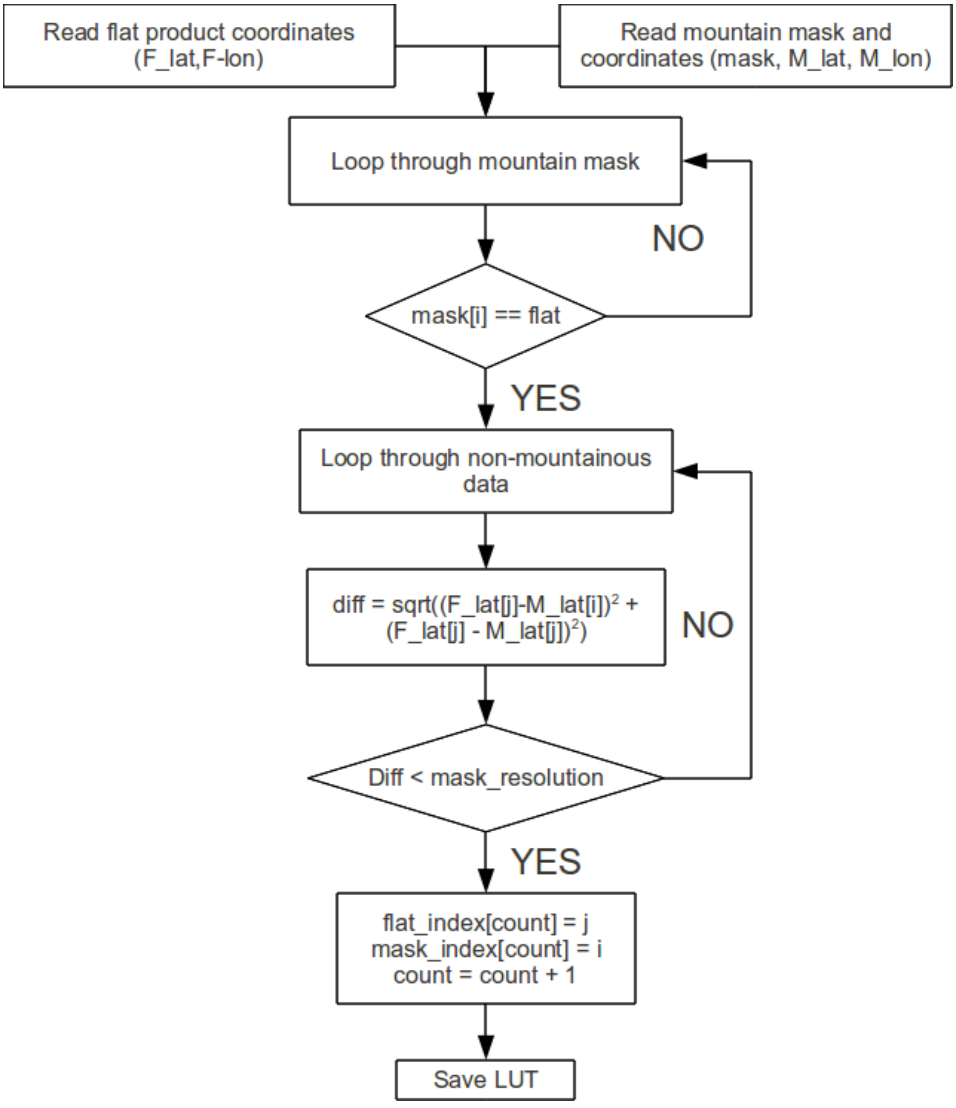

Fig. 13 - Generation of look-up table for merging mountainous and non-mountainous products.

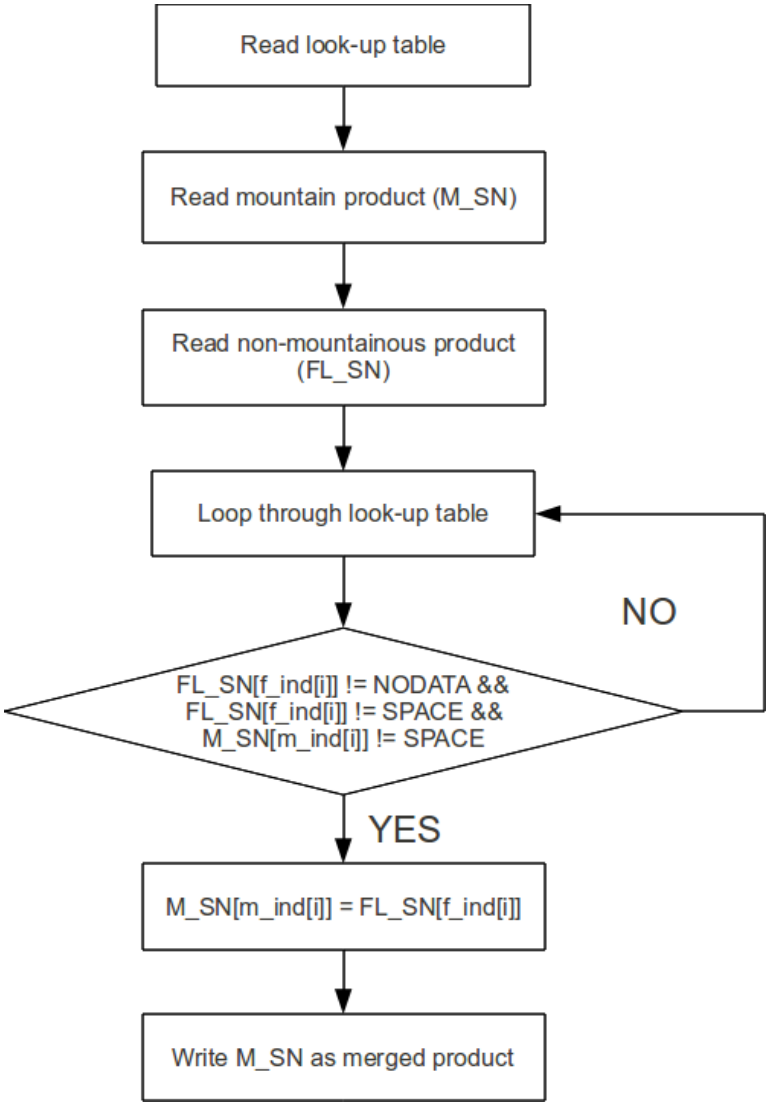

Fig. 14 - Flowchart of snow cover product merging.

5.2 Comparison with the GlobSnow mask [METU]

[*Note - At the SVRR (System Validation Results Review) on 22-23 February 2010 the Board noted that a new mountain mask has been defined in the framework of GlobSnow, an ESA project coordinated by FMI and participated by NR (Norwegian Computing Centre), ENVEO IT GmbH, GAMMA Remote Sensing AG, Finnish Environment Institute (SYKE), Environment Canada (EC) and Northern Research Institute (Norut). The SVRR Board requested H-SAF to perform a comparison between the mountain mask adopted in H-SAF and that one defined by GlobSnow. The study was performed by METU and is reported here below*].

The HSAF and GlobSnow mountain masks have been compared and overlay analyses were made in order to depict the resemblances and differences of two mountain masks over the H-SAF domain (see ***Fig. 15***).

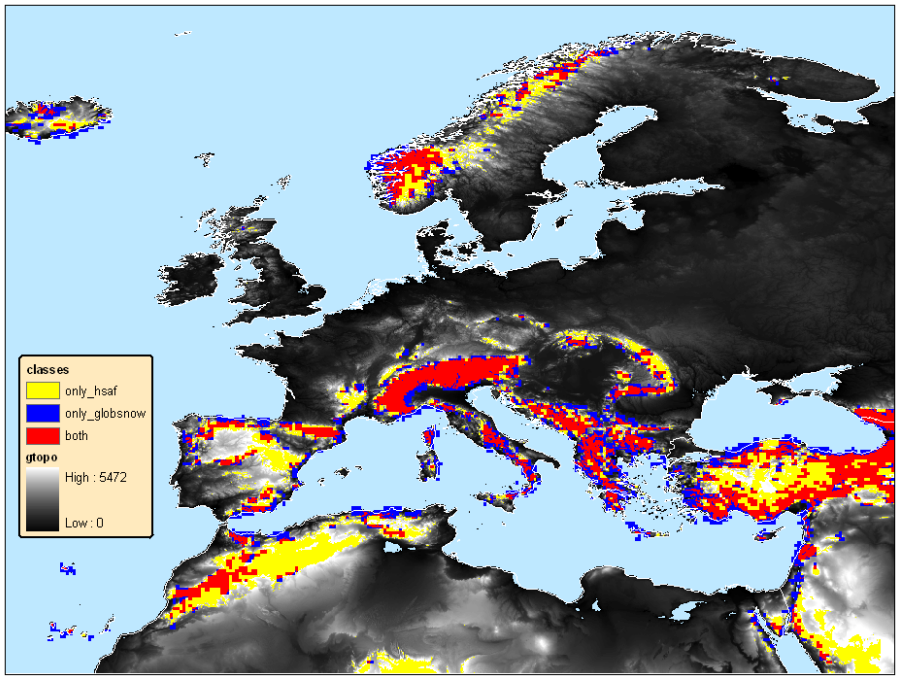

Fig. 15 - The overlay map of HSAF and GlobSnow mountain masks over GTOPO DEM.

At first glance, it could be observed that the common mountain area which is shown with red colour in the figure tells us that there is actually high aliasing between two masks, especially over higher elevations. The resolution of the GlobSnow mountain mask is 25 km since it was formed as EASE Grid format and due to its coarse resolution GlobSnow mountain mask defines mountains with less detail and shows significant amount of mountains over shorelines and sea as well. Some closer views and statistical analyze results are given in ***Fig. 16***, ***Fig. 17*** and ***Fig. 18***.

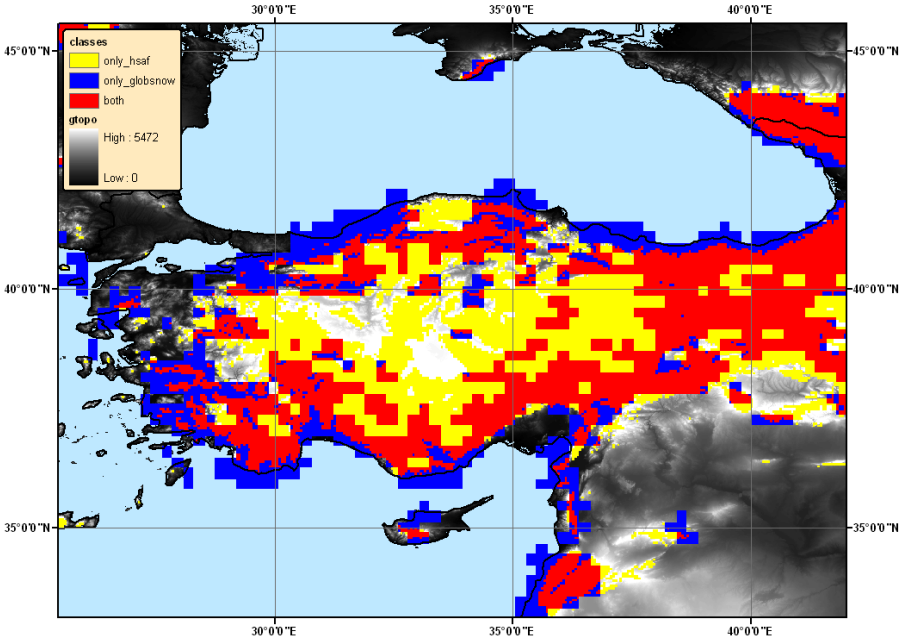

Fig. 16 - Closer view of overlay map focusing Turkey.

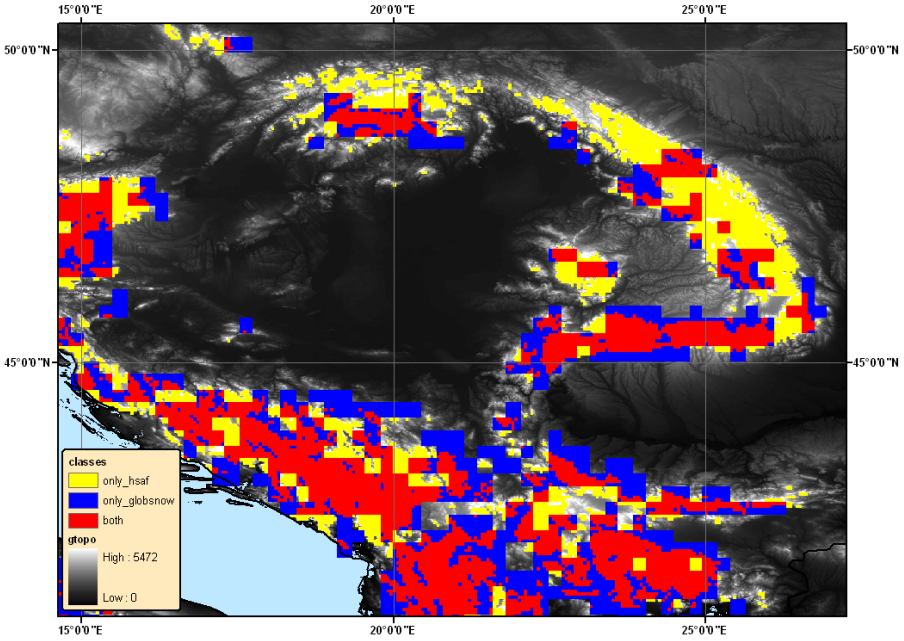

Fig. 17 - Closer view of overlay map focusing Tatra and Carpathian Mountains.

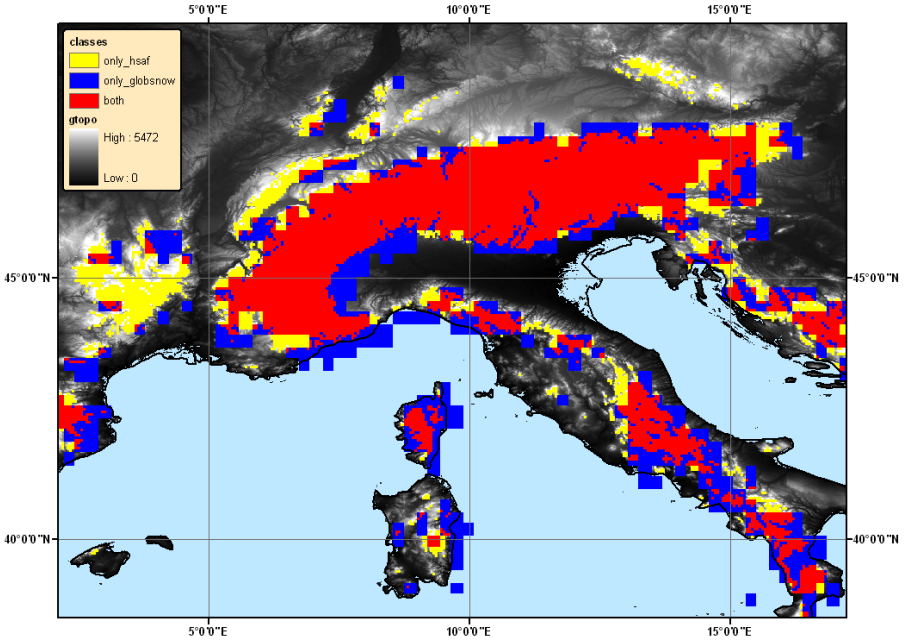

Fig. 18 - Closer view of overlay map focusing Alps.

Statistical scores of the comparisons are reported in ***Table 11*** and ***Fig. 19***.

Table 11 - Statistical results of overlay analysis with GTOPO DEM over Alps

VALUE	INHERIT	PERCENT	MEAN	STD	MEDIAN
1	Only H-SAF	13	919	280	898
2	Only GlobSnow	24	417	278	419
3	Both	63	1500	626	1420

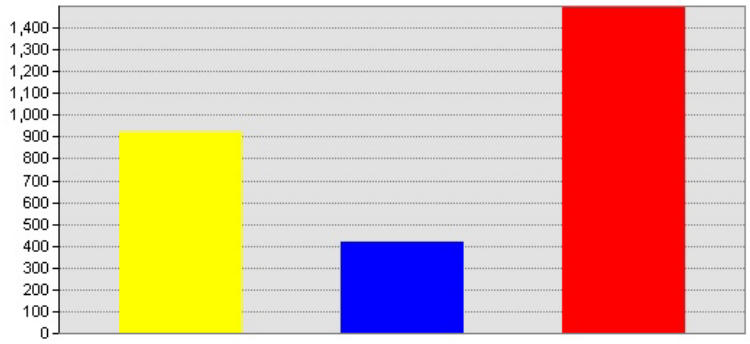

Fig. 19 - The mean values of 3 classes over Alps AOI.

An additional overlay analysis have been applied in order to have an idea about frequency of mountain mask pixels according to elevation zones covering all of the H-SAF domain. The results are given in tabular form in ***Table 12*** and as chart in ***Fig. 20***.

Table 12 - Percentages of mountain mask pixels over elevation zones

Elevation zones (m)	Only H-SAF (%)	Only GlobSnow (%)	Both (%)
0	0.03	21.48	0.08
0-500	1.84	42.68	3.22
500-1000	30.10	31.27	24.22
1000-1500	57.23	3.23	36.19
1500-2000	8.58	1.18	20.26
2000-2500	1.92	0.17	10.81
>2500	0.30	0.00	5.23
Total	100	100	100

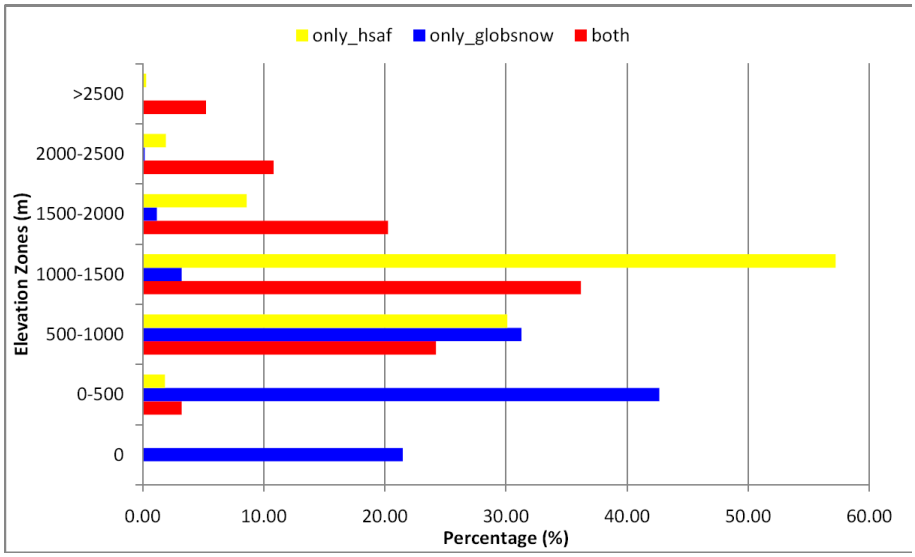

Fig. 20 - The areal distribution of masks over elevation zones.

As it can easily be observed from the figure that most of the pixels belonging to GlobSnow mountain mask are accumulated on lower elevation zones compared with H-SAF mountain mask. Moreover, there is no contribution of GlobSnow mountain mask over 2000 m due to missing high plateaus.

The figures given above analyzing two mountain masks with GTOPO DEM indicate the following additional facts.

Regarding to Fig. 16 which gives a closer view to Turkey, it is seen that the blue colours are mostly covering the areas close to shorelines even extending the land boundaries and overlaps with sea as well. In addition to this, the yellow colours are mostly high plateaus and they are missed by GlobSnow mountain mask which only uses ”Slope > 2°” criteria while on the other hand the H-SAF mountain mask takes some additional parameters into account as it is given below:

"MEAN" ≥ 1000 m

OR

"STD_DEV" ≥ 2 % AND "MEAN" ≥ 700 m

OR

"RANGE" ≥ 800 m AND "MEAN" ≥ 500 m

Related with Fig. 17 that focuses on Tatra and Carpathian Mountains, it clearly shows that the hilly transitional areas are better covered with H-SAF mountain mask for Carpathian.

Finally and most importantly, when Fig. 18 is considered it is easy to observe a big similarity between two maps over main Alps region. On the other hand, some neighbouring mountain areas which are indicated with orange ovals are missed by the GlobSnow mountain mask. While statistical analysis results showed that common mountain areas that has 63 % (red colour) areal coverage with respect to all pixels, has 1500 m mean elevation as expected with a std of 626 m. With the help of additional criteria inclusion in its algorithm, H-SAF mountain mask covers additional 13 % of mountain area which has 919 m mean elevation and 280 m std. However, the blue pixels that are showing the mountain areas that only covered by GlobSnow mountain mask, are hard to be accepted as real mountain areas since they only have 417 m mean elevation and 218 std (also shown on Fig. 20).

The overall recommendation is to keep H-SAF mountain mask for snow products generation.

6. Examples of snow water equivalent maps

At the time of this writing, SN-OBS-4 is generated on a regular basis at FMI and TSMS. An example of map generated by FMI, TSMS, and merged, is provided in ***Fig. 21***.

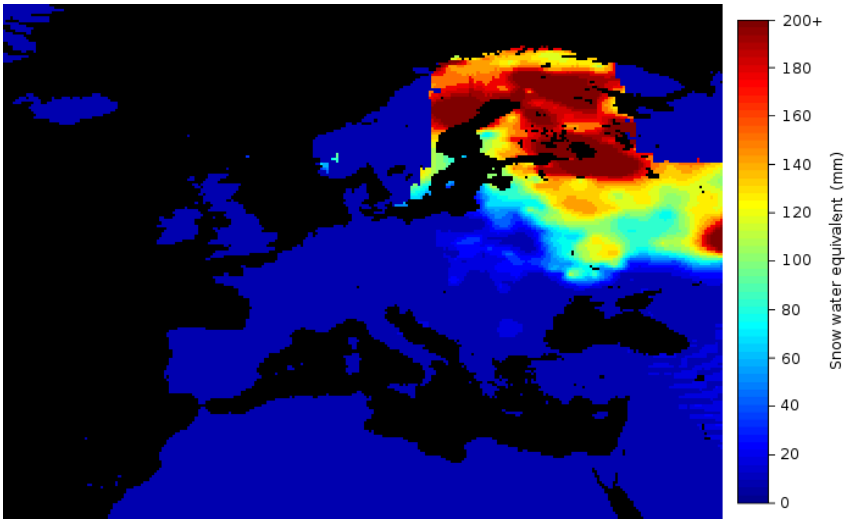

Processed product from FMI, optimised for flat and forested areas.

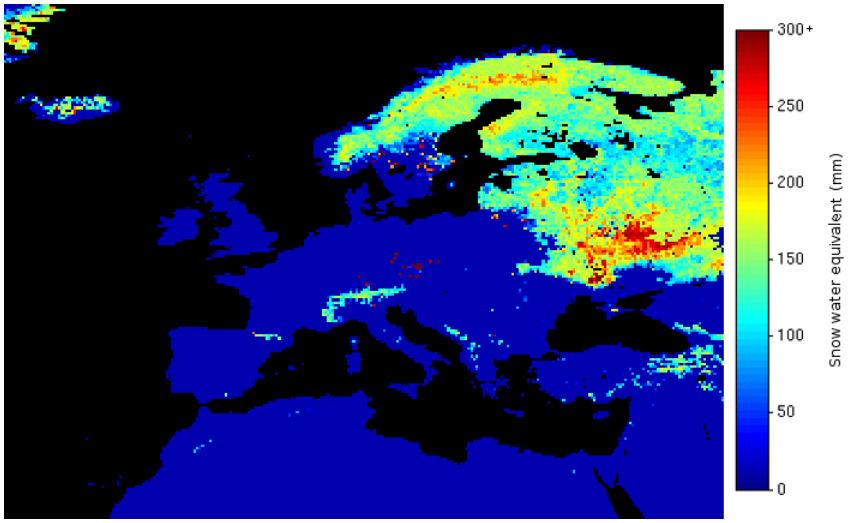

Processed product from TSMS, optimised for mountainous areas.

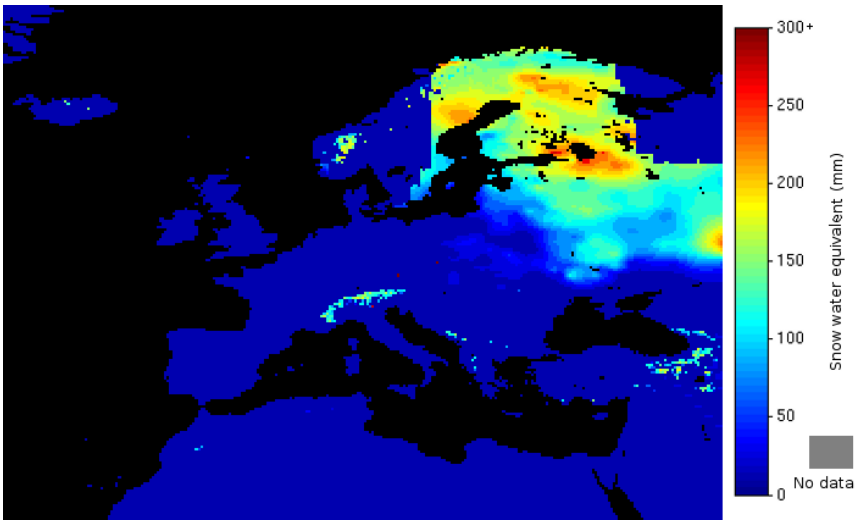

Merged product from FMI and TSMS.

Fig. 21 - Snow water equivalent from EOS-Aqua AMSR-E - Time-composite maps over 24 hours, 18 March 2010.

References

Chang A.T.C., J.L. Foster and D.K. Hall, 1987: "Nimbus-7 SMMR-derived global snow cover parameters". *Ann. Glaciol.*, 9, 39-44.

Ertürk A.G., 2009: "HSAF Visiting Scientist Activity at FMI. Final Report". Hydro-SAF Visiting Scientist Report VS3_11.

Hallikainen M.T., F.T. Ulaby and T.E.V. Deventer, 1987: "Extinction behaviour of dry snow in the 18-to-90 GHz range". *IEEE Transactions on Geoscience and Remote Sensing*, pp. 737-745.

Kärnä J-P., J. Pulliainen, J. Lemmetyinen, M. Hallikainen, P. Lahtinen, and M. Takala, 2007: "Operational Snow Map Production for whole Eurasia using Microwave Radiometer and Ground-based Observations". In *IEEE 2007 International Geoscience and Remote Sensing Symposium (IGARSS'07)*, Barcelona, Spain, July 24 - July 28, 2007.

Kruopis N., J. Praks, A.N. Arslan, H. Alasalmi, J. Koskinen and M. Hallikainen, 1999: "Passive microwave measurements of snow-covered forest areas in EMAC'95". *IEEE Trans. Geosci. Remote Sensing* 37:2699-2705.

Pulliainen J. and M. Hallikainen, 2001: "Retrieval of regional snow water equivalent from space-borne passive microwave observations". *Remote Sensing of Environment*, 75, 76−85.

Pulliainen J., 2006: "Mapping of snow water equivalent and snow depth in boreal and sub-arctic zones by assimilating space-borne microwave radiometer data and ground-based observations". *Remote Sensing of Environment*, 101, 257-269.

Pulliainen J., J. Grandell and M. Hallikainen, 1999: "HUT snow emission model and its applicability to snow water equivalent retrieval". *IEEE Trans. Geosci. Remote Sensing*, 37, 1378−1390.

Pulliainen J., J. Vepsäläinen, S. Kaitala, M. Hallikainen, K. Kallio, V. Fleming and P. Maunula, 2004: "Regional water quality mapping through the assimilation of spaceborne remote sensing data to ship-based transect observations". *J. Geophys. Res.*, 109:C12009, doi:10.1029/2003JC002167.

Pulliainen J., J.-P. Kärnä and M. Hallikainen, 1993: "Development of geophysical retrieval algorithms for the MIMR". *IEEE Trans. Geosci. Remote Sensing*, 31:268-277.

Roy V., K. Goïta, A. Royer, A. Walker and B. Goodison, 2004: "Snow water equivalent retrieval in a Canadian boreal environment from microwave measurements using the HUT snow emission model. IEEE Transactions on Geoscience and Remote Sensing, 42, 1850-1859.